J. Fluid Mech. (2004), *vol.* 508, *pp.* 319–331. © 2004 Cambridge University Press
DOI: 10.1017/S0022112004009206 Printed in the United Kingdom

Transition from Ekman flow to Taylor vortex flow in superfluid helium

By KAREN L. HENDERSON[1] AND CARLO F. BARENGHI[2]

[1]School of Mathematical Sciences, University of the West of England, Bristol BS16 1QY, UK
Karen.Henderson@uwe.ac.uk

[2]School of Mathematics, University of Newcastle, Newcastle upon Tyne NE1 7RU, UK
C.F.Barenghi@ncl.ac.uk

(Received 25 June 2003 and in revised form 2 February 2004)

By numerically computing the steady axisymmetric flow of helium II confined inside a finite-aspect-ratio Couette annulus, we determine the transition from Ekman flow to Taylor vortex flow as a function of temperature and aspect ratio. We find that the low-Reynolds-number flow is quite different to that of a classical fluid, particularly at lower temperatures. At high aspect ratio our results confirm the existing linear stability theory of the onset of Taylor vortices, which assumes infinitely long cylinders.

1. The equations of motion of superfluid helium

As the temperature is reduced through $T = T_\lambda = 2.1768\,\mathrm{K}$, liquid helium undergoes a phase transition from helium I (a classical Navier–Stokes fluid) to helium II (a superfluid). The superfluid state persists through to absolute zero at vapour pressure. The motion of helium II is described well by the hydrodynamic two-fluid theory of Landau (1941) and Tisza (1940). According to this theory, helium II comprises two perfectly mixed fluids, the viscous normal fluid and the inviscid superfluid, of densities ρ^n and ρ^s respectively. The total density of helium II, $\rho = \rho^n + \rho^s$, does not vary much with the temperature T, whereas ρ^n and ρ^s depend strongly on T. At absolute zero, $T = 0\,\mathrm{K}$, the normal fluid component vanishes and helium II is entirely superfluid ($\rho^n = 0$), whilst at the lambda point, $T = T_\lambda$, the superfluid component is zero ($\rho^s = 0$) and helium II becomes helium I, which is a classical Navier–Stokes fluid. If helium II is rotated with angular velocity Ω greater than some small critical value, then vortex filaments appear in the superfluid (Donnelly 1991). The circulation around each vortex filament is quantized, in that

$$\oint_C \boldsymbol{v}^s \cdot \mathrm{d}\boldsymbol{l} = \Gamma \tag{1.1}$$

where $\boldsymbol{v}^s$ is the superfluid velocity field, $\Gamma = 9.97 \times 10^{-4}\,\mathrm{cm^2\,s^{-1}}$ is the quantum of circulation (the ratio of Plank's constant and the mass of one helium atom) and C is an arbitrary integration path around the axis of the filament. When helium II rotates the vortices align themselves to the direction of rotation and form a regular configuration with areal density (number of vortex filaments crossing the unit area perpendicular to the direction of rotation) $N = 2\Omega/\Gamma$ (Feynman's 1955 rule).

The hydrodynamics of the superfluid state is an interesting topic *per se*, but it is worth mentioning that attention to this problem has additional motivations. The first arises from the engineering applications: helium is the only substance available in

liquid form at temperatures near absolute zero, so it is important as a cryogenics coolant. Applications range from infrared detectors in space science to the cooling of superconducting magnets in particle physics. The second motivation comes from recent experimental developments in which the relation between classical and quantum turbulence is investigated (for example see Smith *et al.* 1993; Barenghi, Swanson & Donnelly 1995).

The most generally accepted equations for modelling the macroscopic flow of helium II are the Hall–Vinen–Bekharevich–Khalatnikov (HVBK) equations which were derived by a number of people over the years (Hall & Vinen 1956; Hall 1960; Bekharevich & Khalatnikov 1965; Hills & Robert 1977). These equations extend Landau's two-fluid model to take into account the presence of quantized vortex lines in the flow. The derivation of the equations is based on a continuum approximation, assuming a high density of vortex lines, all aligned roughly in the same direction. For such situations, the superfluid vorticity, which is discrete in nature, may be approximated as a continuum, resulting in an effective superfluid vorticity field $\boldsymbol{\omega}^s = \mathrm{curl}\,\boldsymbol{v}^s$. The isothermal, incompressible HVBK equations may be written as

$$\frac{\partial \boldsymbol{v}^n}{\partial t} + (\boldsymbol{v}^n \cdot \nabla)\boldsymbol{v}^n = -\nabla p^n + \nu^n \nabla^2 \boldsymbol{v}^n + \frac{\rho^s}{\rho}\boldsymbol{F}, \tag{1.2}$$

$$\frac{\partial \boldsymbol{v}^s}{\partial t} + (\boldsymbol{v}^s \cdot \nabla)\boldsymbol{v}^s = -\nabla p^s + \boldsymbol{T} - \frac{\rho^n}{\rho}\boldsymbol{F}, \tag{1.3}$$

$$\nabla \cdot \boldsymbol{v}^n = 0, \quad \nabla \cdot \boldsymbol{v}^s = 0, \tag{1.4}$$

where $\boldsymbol{v}^n$ is the normal fluid velocity, ν^n is the kinematic viscosity of the normal fluid and p^n, p^s are effective pressures ($\nabla p^s = (1/\rho)\nabla p - \frac{1}{2}(\rho^n/\rho)\nabla(\boldsymbol{v}^n - \boldsymbol{v}^s)^2$ and $\nabla p^n = (1/\rho)\nabla p + \frac{1}{2}(\rho^s/\rho)\nabla(\boldsymbol{v}^n - \boldsymbol{v}^s)^2$ where p is the pressure). The mutual friction force may be written as

$$\boldsymbol{F} = \tfrac{1}{2}B\widehat{\boldsymbol{\omega}}^s \times (\boldsymbol{\omega}^s \times (\boldsymbol{v}^n - \boldsymbol{v}^s - \nu^s \nabla \times \widehat{\boldsymbol{\omega}}^s)) + \tfrac{1}{2}B'\boldsymbol{\omega}^s \times (\boldsymbol{v}^n - \boldsymbol{v}^s - \nu^s \nabla \times \widehat{\boldsymbol{\omega}}^s) \tag{1.5}$$

with $\widehat{\boldsymbol{\omega}}^s = \boldsymbol{\omega}^s/|\boldsymbol{\omega}^s|$ the unit vector in the direction of superfluid vorticity and B, B' are the temperature-dependent mutual friction parameters (Barenghi, Donnelly & Vinen 1983; Donnelly & Barenghi 1998). This force is due to collisions between the normal fluid (mainly rotons, at temperatures relevant to most experiments) and vortex lines. The vortex tension force may be written as

$$\boldsymbol{T} = -\nu^s \boldsymbol{\omega}^s \times (\nabla \times \widehat{\boldsymbol{\omega}}^s), \tag{1.6}$$

and reflects the energy per unit length in the vortex lines. The vortex tension parameter

$$\nu^s = (\Gamma/4\pi)\log(b_0/a_0) \tag{1.7}$$

has the same dimension as kinematic viscosity but physically it is very different: it represents the ability of a vortex line to oscillate due to vortex waves which can be excited on the vortex lines themselves. The quantity $b_0 = (|\boldsymbol{\omega}^s|/\Gamma)^{-1/2}$ represents the intervortex spacing and $a_0 \approx 10^{-8}$ cm is the radius of the superfluid vortex core.

2. Motivation and aim of this work

In this paper we apply the HVBK equations to model helium II in a finite-aspect-ratio Couette annulus, that is flow of fluid confined radially between two concentric rotating cylinders and axially between two fixed plates separated by a distance H. We consider the inner cylinder ($r = R_1$) to be rotating with angular velocity Ω_1 and the

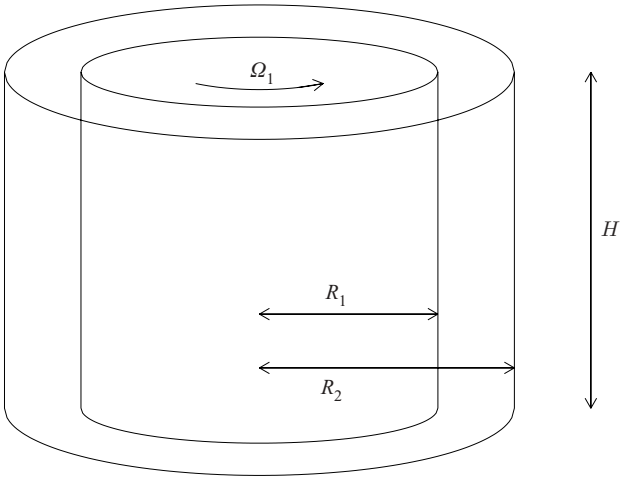

FIGURE 1. The configuration of the problem. The fluid is contained inside a cylindrical box of inner radius R_1, outer radius R_2 and height H. The inner cylinder rotates at constant angular velocity Ω_1, while the outer cylinder and the top and bottom end plates are stationary.

outer cylinder ($r = R_2$) to be fixed, see figure 1. Taylor–Couette flow has been used as a bench-mark for fluid mechanics since Taylor's (1923) pioneering work to investigate the transition from Couette flow to Taylor vortices, which established a firm ground for using the Navier–Stokes equations and the no-slip boundary conditions. Progress in helium II has been slower than for classical fluids due in part to problems of flow visualization at such low temperatures. In considering a classical fluid, introduction of flakes or other small particles into the working fluid (usually oil or water) results in the Taylor vortices being clearly evident. In contrast there are only limited visualization techniques available to the experimentalist at temperatures close to absolute zero. Attempts have been made to reveal the flow pattern of helium II by adding small particles (Bielert & Stamm 1993). However this was only successful at high rotation rates (40 times the critical angular velocity at which linear stability analysis predicts Couette flow becomes unstable); in this regime the flow is turbulent and the validity of the HVBK equations is not clear. Clearly the lack of direct flow visualization gives additional motivation to our work.

Despite the fact that the HVBK equations were established in 1961, they have been used mainly to model helium II in a rotating container (solid body rotation). Unfortunately solid body rotation (which corresponds to a spatially uniform configuration of superfluid vortices) is not a strict test of the equations of motion because it is too simple; the terms in the HVBK equations which involve the vortex tension vanish. Only recently have the HVBK equations been validated for a non-trivial flow configuration: Couette flow. For the case of infinitely long cylinders, both superfluid and normal fluid velocity fields have the following Couette flow profile:

$$\boldsymbol{v}^n = \boldsymbol{v}^s = \frac{\left(-\Omega_1 R_1^2 r + \Omega_1 R_1^2 R_2^2 r^{-1}\right)}{\left(R_2^2 - R_1^2\right)} \widehat{\boldsymbol{\phi}} \tag{2.1}$$

where (r, ϕ, z) are cylindrical coordinates and $\widehat{\boldsymbol{\phi}}$ is the unit vector in the azimuthal direction. After making the usual assumption of infinitely long cylinders, Barenghi & Jones (1988) and Barenghi (1992) considered the linear stability of Couette flow with respect to infinitesimal perturbations of the form $\exp(\mathrm{i}m\phi + \mathrm{i}kz + \sigma t)$ where σ is the

complex growth rate, m the azimuthal wavenumber and k the dimensionless axial wavenumber (expressed in units of $1/\delta$ where $\delta = R_2 - R_1$ is the gap width). The driving parameter of the problem is the Reynolds number,

$$Re = \frac{\Omega_1 R_1 \delta}{\nu^n}, \tag{2.2}$$

which represents the dimensionless velocity of the inner cylinder. Barenghi & Jones (1988) found that if the inner cylinder rotates sufficiently fast, at a certain critical value $Re = Re_{\mathrm{crit}}$ the growth rate, $\mathrm{Re}(\sigma)$ of the axisymmetric ($m = 0$) perturbation becomes positive, hence Couette flow becomes unstable. This transition corresponds to the onset of Taylor vortices for a classical fluid. Barenghi & Jones (1988) also determined the temperature dependence of the critical Reynolds number, Re_{crit}, and of the critical axial wavenumber, k_{crit}. Their work prompted further experiments which were performed by Swanson & Donnelly (1991). They measured the extra attenuation of a second sound wave due to the vortex lines. Second sound waves occur when there is a periodic counterflow between the normal fluid and superfluid, which corresponds to a wave of heat. They plotted the attenuation factor against Reynolds number and found an experimental value for Re_{crit} by considering the break in this curve. Good agreement between the predicted and measured values of Re_{crit} was found (Barenghi 1992), particularly for temperatures close to the lambda point. The success of the linear stability analysis prompted further work, namely the study of nonlinear Taylor flow in infinitely long cylinders (Henderson, Barenghi & Jones 1995). Comparisons with existing experimental data and numerical results further validated the HVBK model in the high-temperature regime (Henderson & Barenghi 1994).

At lower temperatures ($T < 2\,\mathrm{K}$), although there was qualitative agreement, the measured critical Reynolds numbers were larger than those predicted by the linear stability analysis. In the classical Taylor–Couette problem the critical value of the dimensionless axial wavenumber is $k_{\mathrm{crit}} \approx \pi$, hence each individual Taylor vortex cell is approximately square (the extension in the axial direction is equal to the gap's size). In the case of helium II, Barenghi & Jones (1988) found that $k_{\mathrm{crit}} \to \pi$ as $T \to T_\lambda$, as expected in the limit of a pure normal fluid. However, as the temperature is reduced, they found that k_{crit} decreases and tends to zero in the limit of a pure superfluid. This result suggests that the discrepancy between theory and experiments for $T < 2\,\mathrm{K}$ is due to end effects: there are not enough Taylor vortex cells in the typical experimental apparatus, thus the infinite cylinder assumption breaks down. The possibility that vortex pinning at the top and bottom ends may be responsible for the observation should not be neglected, but we prefer not to pursue this line of investigation since it would necessarily introduce arbitrary pinning parameters. Thus in this paper we make an attempt to study the effects introduced by the finite aspect ratio.

It is known in the classical Taylor–Couette literature that the presence of fixed ends induces a large-scale Ekman circulation in which the fluid moves radially inward near the top and bottom ends of the Couette apparatus and moves radially outward in the middle. This effect is caused by the no-slip boundary conditions; the centrifugal force pushes the fluid outwards at the centreline, where the braking effect of the end plates is least, so the fluid near the end plates moves inwards to conserve mass. In the case of helium II the normal fluid obeys the same no-slip boundary condition as an ordinary classical fluid, but there are also superfluid boundary conditions to take into account. A discussion of what these superfluid boundary conditions should be is contained in our previous paper (Henderson & Barenghi 2000), in which we also showed that the competition between the normal fluid and superfluid boundary

conditions has unexpected effects on the direction of rotation of the Ekman circulation in a unit-aspect-ratio annulus. The aim of the current paper is to understand how the appearance of Taylor vortex flow is affected by the underlying Ekman circulation. First we shall investigate the low-Reynolds-number flow of helium II at varying aspect ratios to see how it differs from the flow of a classical Navier–Stokes fluid. Secondly, we shall determine the transition from Ekman cells to Taylor vortices and compare the Taylor–Couette flow of helium II in an enclosed annulus to the flow in an infinite apparatus (Henderson *et al.* 1995). If, for sufficiently long cylinders, the results of the linear stability theory are recovered, contact will have been made between theory and experiments at low temperatures.

3. Model

We consider the fluid to be confined radially between two concentric cylinders of inner and outer radius R_1 and R_2 respectively, and axially between two fixed plates which are separated by a distance H. The top and bottom plates and the outer cylinder are held stationary and the inner cylinder rotates at constant angular velocity Ω_1. Throughout this work we shall consider the radius ratio, $\eta = R_1/R_2 = 0.976$ as in the experimental apparatus of Swanson & Donnelly (1991) and will vary the Reynolds number, $Re = \Omega_1 R_1 \delta/\nu^n$, the aspect ratio, $h = H/\delta$ and the temperature, T. The aspect ratio of the experimental apparatus used by Swanson & Donnelly (1991) was $h = 199$; we are constrained numerically and the largest value of aspect ratio at which we are able to compute converged numerical solutions is $h = 8$.

In order to solve the HVBK equations (1.2)–(1.4) we need boundary conditions. The boundary conditions for the normal fluid are no-slip, that is, working in cylindrical coordinates, $\boldsymbol{v}^n = \Omega_1 R_1 \widehat{\boldsymbol{\phi}}$ at $r = R_1$ and $\boldsymbol{v}^n = 0$ at $r = R_2$, $z = 0$, $z = H$. The boundary conditions for the superfluid are more delicate. Given $\boldsymbol{n}$, a normal to the boundary, we have that $\boldsymbol{v}^s \cdot \boldsymbol{n} = 0$ at $r = R_1, R_2$ and $z = 0, H$, ensuring no flow normal to the boundaries. For the remaining conditions we have taken

$$\boldsymbol{\omega}^s \times \widehat{z} = 0 \quad \text{at} \quad r = R_1, R_2 \quad \text{and} \quad z = 0, H, \tag{3.1}$$

where $\widehat{z}$ is the unit vector in the axial direction. Thus the superfluid vorticity is taken to be purely axial at the boundaries. The condition on the cylinder walls, $r = R_1$ and $r = R_2$, has been discussed in a previous paper (Henderson *et al.* 1995) whilst the condition on the ends of the cylinder, $z = 0$ and $z = H$, corresponds to perfect sliding of the vortex lines (Khalatnikov 1965). It must be stressed that as yet there is no experimental evidence for the boundary conditions which we propose; in fact, a motivation behind our work is to explore the consequence of assuming certain boundary conditions, hoping to stimulate experimental work on this issue.

For rotation of the inner cylinder only, linear stability analysis predicts that the axisymmetric mode onsets first (Barenghi & Jones 1988). We have no direct information from the experiments about the Reynolds number at which non-axisymmetric motion appears, hence we choose to make the simplifying assumption that the flow is axisymmetric and introduce stream functions ψ^n, ψ^s such that

$$v_r^p = -\frac{1}{r}\frac{\partial \psi^p}{\partial z}, \qquad v_z^p = \frac{1}{r}\frac{\partial \psi^p}{\partial r} \tag{3.2a,b}$$

where $p = n$, s represents the normal fluid, superfluid respectively. Introducing the stream functions ensures that continuity (1.4) is automatically satisfied. A finite difference approach is used to obtain solutions for ψ^p, v_ϕ^p and ω_ϕ^p at each time step.

The equations satisfied by v_ϕ^p, ω_ϕ^p are obtained by taking the ϕ component of (1.2), (1.3) and the ϕ component of the curl of (1.2), (1.3). These equations are stepped forward in time until a steady solution is achieved. The initial conditions are taken to be either a very small seed field or a steady solution previously obtained at some other values of the input parameters. A Poisson's equation links the stream function ψ^p with the azimuthal component of vorticity ω_ϕ^p and this is updated at each time-step. The computational domain is $R_1 \leqslant r \leqslant R_2$, $0 \leqslant z \leqslant H/2$ and symmetry is assumed to calculate the derivatives on the centreline $z = H/2$. The decision to restrict solutions to those with Z_2 symmetry was made in order to improve the numerical resolution near the end plates. Before restricting the symmetry in this way, low-resolution runs did not detect any solution in which the symmetry was broken in the range of parameters used. In the classical Couette problem at short aspect ratio it is known that asymmetric solutions exist (Pfister *et al.* 1988). However these solutions occur at Reynolds numbers higher than the values which we have investigated. A uniform grid is used in both the radial and axial direction. For all the results presented 16 mesh points are used in the radial direction and $16 \times h$ in the axial direction, which is sufficient to achieve numerical convergence and is consistent with Pfister *et al.* (1988). The equations are made dimensionless using the gap width δ as the unit of length and the normal fluid viscous time scale δ^2/ν^n as the unit of time. For further details of the numerical method, see Henderson & Barenghi (2000).

4. Results

In this section we refer to previous results (Henderson & Barenghi 2000) in which we considered the low-Reynolds-number flow of helium II in a unit-aspect-ratio Couette annulus; this geometry constrains the flow to a simple Ekman circulation. The key discovery was the anomalous Ekman motion of helium II, compared to a classical Navier–Stokes fluid. We found that the pair of superfluid Ekman cells always rotates in a counter-classical direction (which means for example that $v_r^s < 0$ at the centreline $z = H/2$). This result was explained by considering the azimuthal component of the steady form of equations (1.2) and (1.3) on the end plates $z = 0, H$. It was found that $v_r^s > 0$ on $z = 0, H$ due to the mutual friction term. The normal-fluid Ekman cells were found to rotate classically ($v_r^n > 0$ at $z = H/2$) at temperatures close to the lambda temperature, but to reverse ($v_r^n < 0$ at $z = H/2$) at lower temperatures. This phenomenon may be explained by looking at the mutual friction term in equation (1.2). As the temperature approaches T_λ the superfluid fraction ρ^s/ρ decreases rapidly; thus equation (1.2) becomes the Navier–Stokes equation and the normal fluid behaves classically. However as the temperature decreases away from T_λ the relative importance of the mutual friction term increases and the normal fluid is dragged along by the superfluid in a counter-classical direction. It was also found that the azimuthal superfluid velocity is almost independent of z. This effect becomes more pronounced at lower temperatures and was found to be due to the tension in the superfluid vortex lines.

In this paper, the parameters which are varied are the temperature T, Reynolds number Re of the inner cylinder and aspect ratio h. Figures 2–4,6 show contour plots of the normal and superfluid stream functions, where the plots are shown for the complete cross-section of the annulus: $R_1 \leqslant r \leqslant R_2$, $0 \leqslant z \leqslant H$ with the inner/outer cylinder on the left/right respectively. The maximum value of each field is printed underneath the corresponding contour plot. Solid and dashed lines correspond to positive and negative contour lines respectively.

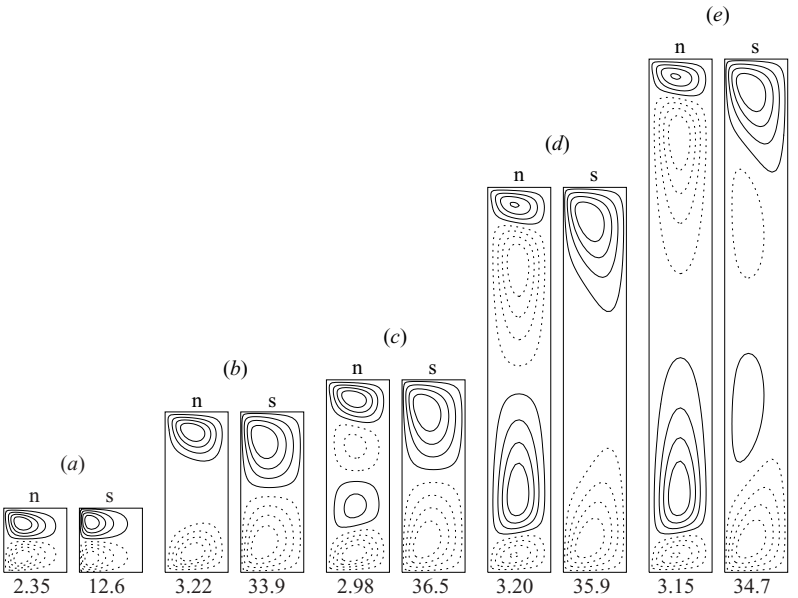

FIGURE 2. Contour plots of the stream function of the normal fluid (n) and the superfluid (s) at $T = 2.11$ K and $Re = 100$ at aspect ratios: (*a*) $h = 1$, (*b*) $h = 2.5$, (*c*) $h = 3$, (*d*) $h = 6$, (*e*) $h = 8$.

In figure 2 we investigate how varying the aspect ratio affects the flow of helium II at $T = 2.11$ K and $Re = 100$. This Reynolds number is appreciably below the critical Reynolds number ($Re_{\mathrm{crit}} = 355$) at which the linear stability analysis predicts Couette flow becomes unstable in the infinite cylinder approximation. It is apparent from figure 2(*a*) that since the normal fluid and superfluid stream functions increase with z across the centreline $z = H/2$, (3.2*a*) predicts that the radial velocity components are negative at the centreline, in contrast to the motion of a classical Navier–Stokes fluid. Thus for small aspect ratios ($h \leqslant 2.5$) both the normal fluid and superfluid rotate counter-classically in a pair of matching Ekman cells. This behaviour has been reported previously (Henderson & Barenghi 2000) and is due to the boundary conditions satisfied by the vortex lines on the top and bottom of the cylinders. Figure 2 also shows that the superfluid Ekman cells fill the whole annulus, becoming more elongated as the aspect ratio is increased. In contrast, the normal-fluid Ekman cells, tend to retain their size and are positioned towards the ends of the cylinders.

As the aspect ratio is increased further ($h > 2.5$) the superfluid remains in the form of two counter-rotating cells whilst the normal fluid splits into four cells with the cells adjacent to the ends of the cylinder rotating in the same direction as the superfluid. The inner cells of the normal fluid strengthen and fill the annulus as the aspect ratio is increased. At aspect ratio $h = 8$ the superfluid splits into four cells and although the size of the cells is different to those of the normal fluid, the direction of rotation is the same for both fluids.

Taken together these results demonstrate that the low-Reynolds-number flow of helium II is dominated by end effects, which force the outer cells of the normal and superfluid to rotate counter-classically. As the aspect ratio is increased the influence of the ends at the centre of the apparatus becomes weaker and classical behaviour is observed in both fluids, with outflow at the centreline, $z = H/2$. In our previous work

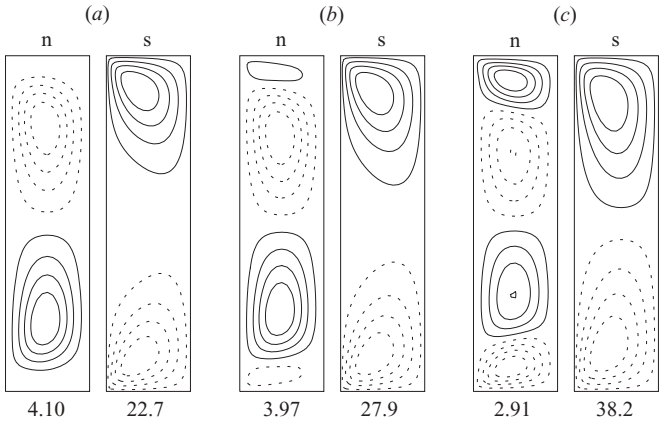

FIGURE 3. Contour plots of the stream function of the normal fluid (n) and the superfluid (s) at $Re = 100$ and $h = 4$ at temperatures: (*a*) $T = 2.16$ K, (*b*) $T = 2.15$ K, (*c*) $T = 2.1$ K.

(Henderson & Barenghi 2000) we highlighted the columnar motion of the azimuthal component of superfluid velocity. We find that as the aspect ratio is increased this column-like motion becomes less pronounced.

In figure 3 we show how varying the temperature affects the flow of helium II at $Re = 100$ and $h = 4$. At this aspect ratio, the maximum axial wavelength of a disturbance is $\lambda_{\max} = 4$ giving a corresponding minimum admissible axial wavenumber of $k_{\min} = \pi/2$. Given this, the Reynolds number, $Re = 100$ is below the critical value, predicted by linear stability analysis, at which Couette flow becomes unstable for all temperatures considered. At temperatures close to the lambda temperature ($T \geqslant 2.16$ K) the normal fluid and superfluid rotate in a pair of Ekman cells. The normal fluid rotates in a classical direction and the superfluid rotates counter-classically. As the temperature is reduced the normal fluid splits into four cells, whilst the superfluid remains as two cells. In this region, the normal fluid cells closest to the ends of the cylinder rotate in the same direction as the superfluid and become stronger in magnitude and also fill more of the annulus as the temperature is reduced. The columnar behaviour of the azimuthal superfluid velocity is not evident at temperatures close to the lambda temperature but becomes more pronounced as the temperature is reduced.

In figure 4 we investigate the transition from Ekman flow to Taylor vortex flow at $T = 2.17$ K and $h = 6$. At low Reynolds numbers ($Re = 100$) the normal fluid consists of a pair of classically rotating Ekman cells. The superfluid has four cells, with the cells adjacent to the ends of the cylinders rotating counter-classically. As the Reynolds number is increased both the normal fluid and the superfluid develop more cells, with the cells closest to the ends rotating classically and counter-classically for the normal and superfluid respectively, as predicted by Henderson & Barenghi (2000). This development of cellular motion spreads from the ends of the annulus as is observed for a classical fluid. At $Re = 300$ Taylor vortex flow is fully developed and we can see that despite the superfluid having an additional weak pair of cells close to the ends of the cylinders, the two fluids appear to match each other. In figure 5 we plot the centreline average values of the radial components of the normal fluid (solid) and superfluid (dashed) against Reynolds number. Stability analysis in the infinitely long cylinders approximation predicts $Re_{\text{crit}} = 278.7$ at $k_{\text{crit}} = 2.9$. When the ends of the cylinders are included in the classical Taylor–Couette problem the bifurcation at

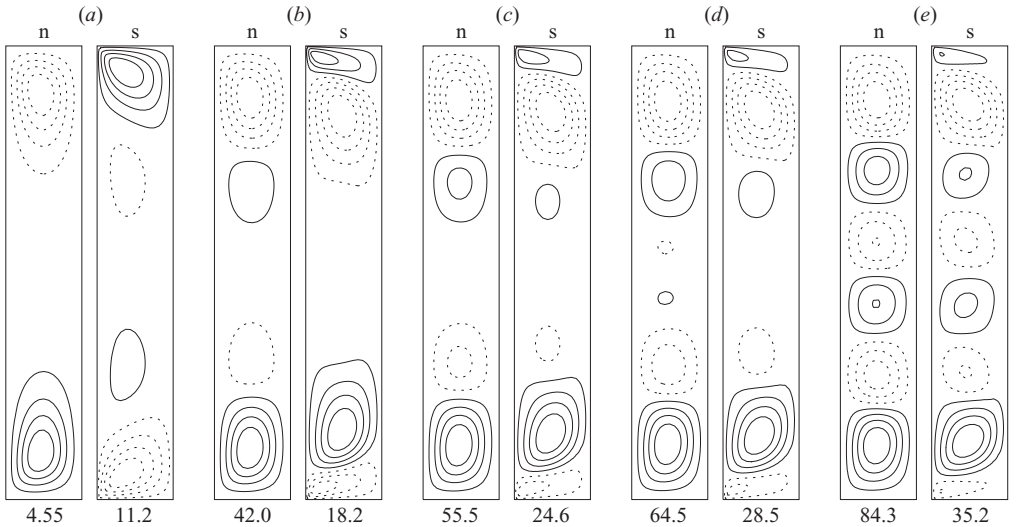

FIGURE 4. Contour plots of the stream function of the normal fluid (n) and the superfluid (s) at $T = 2.17\,\mathrm{K}$ and $h = 6$ at Reynolds numbers: (*a*) $Re = 100$, (*b*) $Re = 250$, (*c*) $Re = 270$, (*d*) $Re = 280$, (*e*) $Re = 300$.

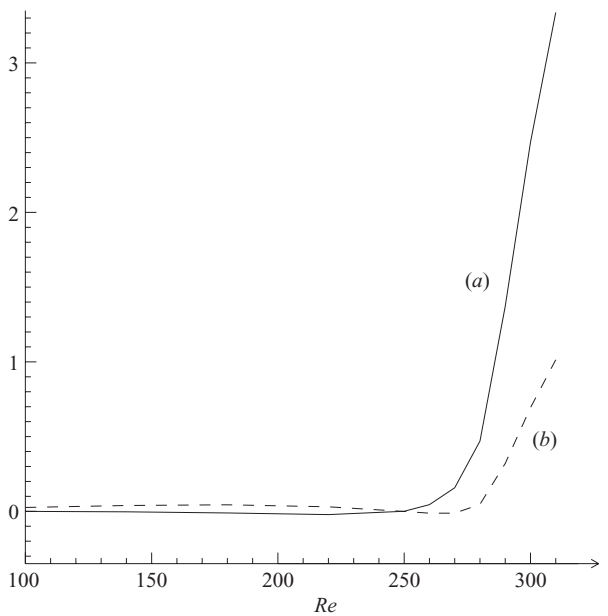

FIGURE 5. Plot of the average values of (*a*) v_r^n (solid) and (*b*) v_r^s (dashed) at the centreline $z = H/2$ against Reynolds number at $T = 2.17\,\mathrm{K}$.

Re_{crit} is imperfect. We can see from figure 5 that this is also the case for helium II. The normal fluid develops Taylor vortices throughout the annulus at a slightly lower Reynolds number than for the superfluid but the value of Re for which both fluids display fully developed Taylor vortices is consistent with linear theory.

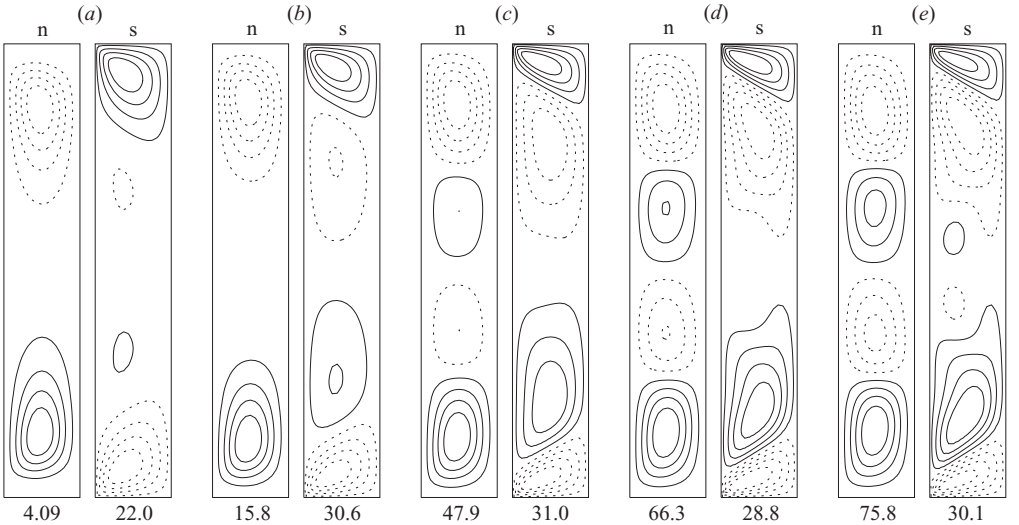

FIGURE 6. Contour plots of the stream function of the normal fluid (n) and the superfluid (s) at $T = 2.16\,\mathrm{K}$ and $h = 6$ at Reynolds numbers: (*a*) $Re = 100$, (*b*) $Re = 180$, (*c*) $Re = 275$, (*d*) $Re = 300$, (*e*) $Re = 310$.

In figure 6 we repeat the calculation at $h = 6$ but setting a lower temperature, $T = 2.16\,\mathrm{K}$. At low Reynolds numbers ($Re = 100$) the normal fluid has a pair of classically rotating Ekman cells. As before, the superfluid has four cells, and the cells which are adjacent to the ends of the cylinders rotate counter-classically. As the Reynolds number is increased, the normal fluid develops four cells which fill the whole apparatus, not six as at $T = 2.17\,\mathrm{K}$. The superfluid remains as four cells up to $Re = 300$, with the outer cells rotating counter-classically and the inner cells strengthing with increasing Reynolds number. At $Re = 310$ the superfluid develops an additional small weak pair of cells at the centre of the apparatus.

In figure 7 we plot the centreline average values of the radial components of the normal fluid (solid) and superfluid (dashed) against Reynolds number. At $T = 2.16\,\mathrm{K}$ the transition from Ekman flow to fully developed Taylor vortices is less sharp than at higher temperatures. Again the normal fluid develops Taylor vortices at a lower Reynolds number than for the superfluid. By considering the point at which $v_r^s(z = H/2)$ becomes positive, we can see that the superfluid develops six cells at $Re = 300$. What is interesting about these results is that the Taylor vortices for the normal fluid are elongated, being $1\frac{1}{2}$ times longer than they are wide. This is consistent with the linear stability analysis which predicts that $Re_{\mathrm{crit}} = 310.68$ at the critical axial wavenumber of $k_{\mathrm{crit}} = 2.35$. The elongation of the Taylor cells was first predicted by Barenghi & Jones (1988) and this is the first time that it has been observed numerically taking end effects into account. It is clear by looking at the superfluid in figure 6(*e*) that the flow is dominated by end effects and in order to obtain quantitative agreement with Re_{crit} as predicted by the linear theory a larger aspect ratio needs to be considered.

We find that in general the superfluid vorticity is primarily axial and concentrated towards the ends of the cylinders close to the inner cylinder. This predicted result could be observed experimentally by measuring the extra attenuation of second sound waves due to the vortex lines at the centre and ends of the apparatus. As the Reynolds

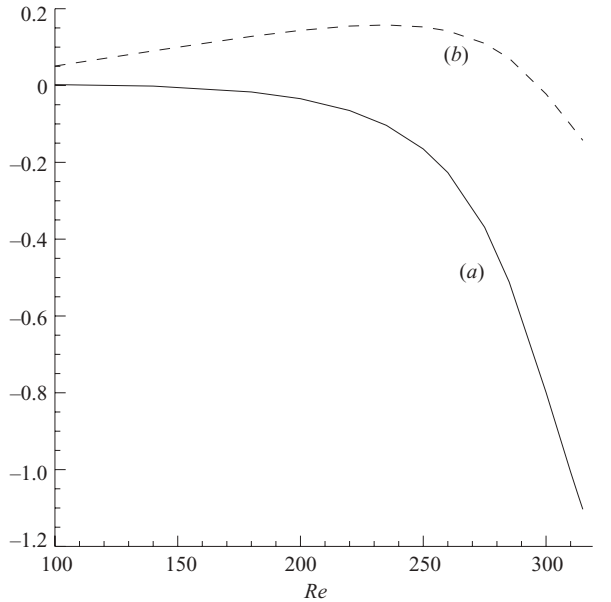

FIGURE 7. Plot of the average values of (*a*) v_r^n (solid) and (*b*) v_r^s (dashed) at the centreline $z = H/2$ against Reynolds number at $T = 2.16\,\mathrm{K}$.

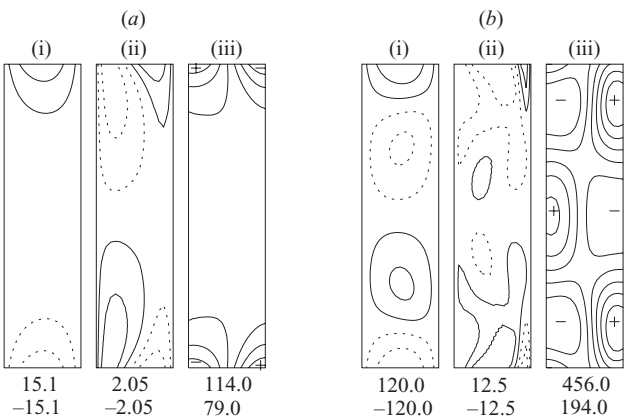

FIGURE 8. Contour plots of the components of superfluid vorticity: (i) ω_r^s, (ii) ω_ϕ^s, (iii) $-\omega_z^s$, at $T = 2.16\,\mathrm{K}$, $h = 6$ for (*a*) $Re = 100$, (*b*) $Re = 300$ in the middle two-thirds of the annulus, $1 \leqslant z/\delta \leqslant 5$. The maximum and minimum values of each field are printed underneath the corresponding plot.

number is increased, there is a much larger deflection of the vortex lines in the radial direction. This deflection has been observed experimentally in the transition to Taylor vortices (Swanson & Donnelly 1991). In figure 8 we plot the superfluid vorticity components of helium II at $T = 2.16\,\mathrm{K}$, $h = 6$ at the Reynolds numbers (*a*) $Re = 100$ and (*b*) $Re = 300$ for the middle two-thirds of the apparatus ($1 \leqslant z/\delta \leqslant 5$). This enables us to see what happens to the vortex lines in the centre of the apparatus away from the cylinder ends, where there is stronger shear which would make the contour lines in the middle of the apparatus less visible. The deflection in the radial direction is clearly visible for $Re = 300$. In the Taylor vortex flow regime, the vorticity pattern is

similar to that found when considering the Taylor–Couette flow of helium II without end effects (Henderson *et al.* 1995).

5. Conclusions

By solving the steady axisymmetric form of the nonlinear HVBK equations in a finite-aspect-ratio configuration we have determined how the fixed ends of the cylinders affect the Ekman flow and the transition to Taylor vortex flow.

For low-Reynolds-number flow, the main result is the anomalous Ekman circulation of helium II when compared to that of a classical Navier–Stokes fluid. At short aspect ratios both normal fluid and superfluid rotate as a pair of Ekman cells. The superfluid cells always rotate counter-classically, whilst the sense of rotation of the normal fluid is temperature dependent. At larger aspect ratios the influence of the ends of the cylinders diminishes towards the centre of the apparatus and at lower temperatures the normal fluid develops additional cells resulting in classical outflow at the centreline. The superfluid also develops extra cells to match the flow of the normal fluid at the centre.

We have found that at $T = 2.17\,\mathrm{K}$ and aspect ratio as small as $h = 6$, in the regions way from the ends of the cylinders, the superfluid's pattern matches that of the normal fluid. The transition to Taylor vortex flow occurs at a Reynolds number close to that predicted by the linear stability analysis in the infinite cylinder approximation. At the slightly lower temperature of $T = 2.16\,\mathrm{K}$ we find that the normal fluid develops elongated Taylor cells, as predicted by the linear stability analysis. The superfluid flow pattern is similar to that of the normal fluid away from the ends of the cylinders but the matching is not as pronounced as at higher temperatures.

Finally we note that gaining more insight into the flow of helium II is particularly worthwhile because of the lack of direct flow visualization at temperatures close to absolute zero.

REFERENCES

Barenghi, C. F. 1992 Vortices and the Couette flow of helium II. *Phys. Rev.* B **45**, 2290–2293.

Barenghi, C. F., Donnelly, R. J. & Vinen, W. F. 1983 Friction on quantized vortices in He II. A review. *J. Low Temp. Phys.* **52**, 189–247.

Barenghi, C. F. & Jones, C. A. 1988 The stability of the Couette flow of helium II. *J. Fluid Mech.* **197**, 551–569.

Barenghi, C. F., Swanson, C. J. & Donnelly, R. J. 1995 Emerging issues in helium turbulence. *J. Low Temp. Phys.* **100**, 385–413.

Bekharevich, I. L. & Khalatnikov, I. M. 1961 Phenomenological derivation of the equations of vortex motion in He II. *Sov. Phys. JETP* **13**, 643–646.

Bielert, F. & Stamm, G. 1993 Visualisation of Taylor Couette flow in superfluid helium. *Cryogenics* **33**, 938–940.

Donnelly, R. J. 1991 *Quantized Vortex Lines in Helium II*. Cambridge University Press.

Donnelly, R. J. & Barenghi, C. F. 1998 The observed properties of liquid helium at the saturated vapour pressure. *J. Phys. Chem. Ref. Data* **27**, 1217–1274.

Feynman, R. P. 1955 Application of quantum mechanics to liquid helium. In *Progress in Low Temperature Physics*, vol. 1 (ed. C. J. Gorter). North Holland.

Hall, H. E. 1960 The rotation of liquid helium II. *Adv. Phys.* **9**, 89–146.

Hall, H. E. & Vinen, W. F. 1956 The rotation of liquid He II. II the theory of mutual friction in uniformly rotating He II. *Proc. R. Soc. Lond.* A **238**, 215–234.

Henderson, K. L. & Barenghi, C. F. 1994 Calculation of the torque in nonlinear Taylor vortex flow of helium II. *Phys. Lett.* A **191**, 438–442.

Henderson, K. L. & Barenghi, C. F. 2000 The anomalous motion of superfluid helium in a rotating cavity. *J. Fluid Mech.* **406**, 199–219.

Henderson, K. L., Barenghi, C. F. & Jones, C. 1995 Nonlinear Taylor-Couette flow of helium II. *J. Fluid Mech.* **283**, 329–340.

Hills, R. N. & Roberts, P. H. 1977 Superfluid mechanics for a high density of vortex lines. *Arch. Rat. Mech. Anal.* **66**, 43–71.

Kapitza, P. L. 1941 The study of heat transfer in helium II. *J. Phys. USSR* **4**, 181–210.

Khalatnikov, I. M. 1965 *An Introduction to the Theory Superfluidity*. Benjamin.

Landau, L. D. 1941 The theory of superfluidity of helium II. *J. Phys. USSR* **5**, 71.

Pfister, G., Schmidt, H., Cliffe, K. A. & Mullin, T. 1988 Bifurcation phenomena in Taylor–Couette flow in a very short annulus. *J. Fluid Mech.* **191**, 1–18.

Smith, M. R., Donnelly, R. J., Goldenfeld, N. & Vinen, W. F. 1993 Decay of vorticity in homogeneous turbulence. *Phys. Rev. Lett.* **71**, 2583–2586.

Swanson, C. J. & Donnelly, R. J. 1991 Instability of Taylor-Couette flow of helium II. *Phys. Rev. Lett.* **67**, 1578–1581.

Taylor, G. I. 1923 Stability of a viscous liquid contained between two rotating cylinders. *Phil. Trans. R. Soc. Lond.* A **223**, 289–343.

Tisza, L. 1938 Transport phenomena in helium II. *Nature* **141**, 913.